SOLAR RADIATION PRESSURE ESTIMATION AND ANALYSIS OF A GEO CLASS OF HIGH AREA-TO-MASS RATIO DEBRIS OBJECTS

Tom Kelecy[*], Tim Payne[†], Robin Thurston[‡] and Gene Stansbery[§]

A population of deep space objects is thought to be high area-to-mass ratio (AMR) debris having origins from sources in the geosynchronous orbit (GEO) belt. The typical AMR values have been observed to range anywhere from 1's to 10's of m^2/kg, and hence, higher than average solar radiation pressure effects result in long-term migration of eccentricity (0.1-0.6) and inclination over time. However, the nature of the debris orientation-dependent dynamics also results time-varying solar radiation forces about the average which complicate the short-term orbit determination processing. The orbit determination results are presented for several of these debris objects, and highlight their unique and varied dynamic attributes. Estimation or the solar pressure dynamics over time scales suitable for resolving the shorter term dynamics improves the orbit estimation, and hence, the orbit predictions needed to conduct follow-up observations.

INTRODUCTION

Background

A population of deep space objects is thought to be debris having origins from sources in the geosynchronous orbit (GEO) belt. There is a heightened interest in the international community due to the large number and small size of these objects, as they pose a hazard to active satellites operating in the vicinity of the GEO belt. The longitudinal migration, along with the dimness and variability of the visual magnitudes make them a challenge to track consistently. Their apparent small size makes this debris a dim optical target, and at GEO ranges, nearly impossible to track with radar. Nevertheless, repeat tracking is paramount to making long-term observations with other sensors that will allow better characterization of the material makeup of these objects, and provide long-term orbital histories that might allow the debris to be tied to specific breakup events or objects of origin.

[*] Senior Scientist, Boeing LTS / AMOS, Kihei, HI and Colorado Springs, CO
[†] Air Force Space Command / A9AC, Colorado Springs, CO
[‡] 1st Space Control Squadron / DOMA, Colorado Springs, CO
[§] NASA/Johnson Space Center, Orbital Debris Program Office, Houston, TX

It has been hypothesized that this class of debris originated from thermal insulation (e.g. MLI), or similar materials. Observational coverage of these objects has been limited by the orbital phasing and the locations of the tracking sites. Boeing, NASA and the U.S. Air Force Space Command have embarked on a collaborative effort with the Inter-Agency Space Debris Coordination Committee (IADC) to track selected high AMR of this population to more accurately characterize their orbits and orbit histories. Space Command tracking assets have been tasked to provide angles measurements for representative set of high AMR debris objects, and the data were used to update the orbits, including estimation of AMR, and to provide a source for predictions to support follow-up observations.

Long-term Effects from Solar Radiation Pressure Perturbations

Analysis has been conducted[1,2] indicating that these objects have area-to-mass ratios (AMR's) averaging anywhere from 1's to 10's of m^2/kg, and thus explains observed migration of eccentricity (0.1-0.6) and inclination that distinguishes their orbital characteristics. To illustrate this, the solar radiation perturbation effects on orbital period, inclination and eccentricity over a 20 year period are shown in the Figures 1, 2 and 3 for AMR's of 0.01, 1, 10 and 20 m^2/kg. The amplitudes and periods of the perturbations vary according to the AMR.

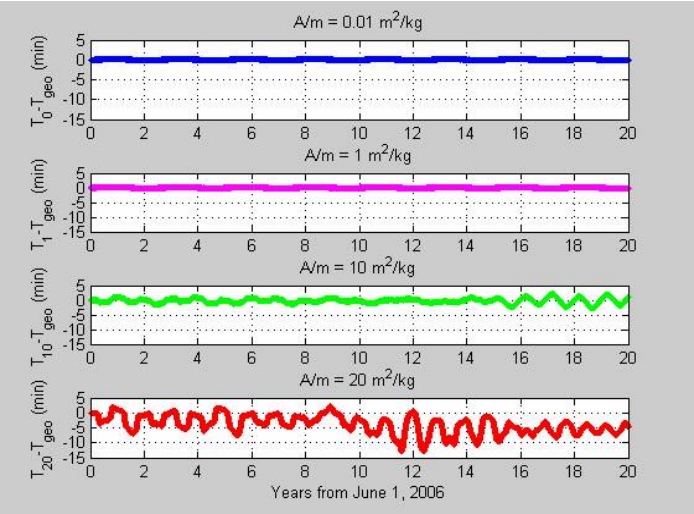

Figure 1 Deviation from GEO Period 20-year Histories for A/m = .01, 1, 10 and 20 m^2/kg

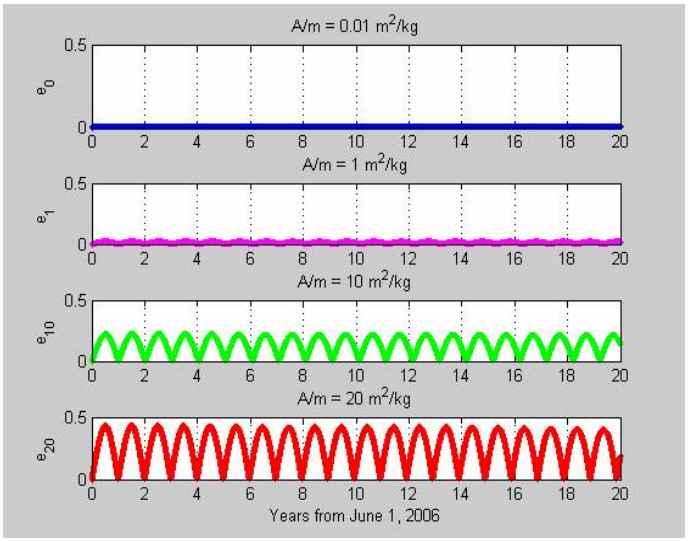

Figure 2 Eccentricity 20-year Histories for A/m = .01, 1, 10 and 20 m^2/kg

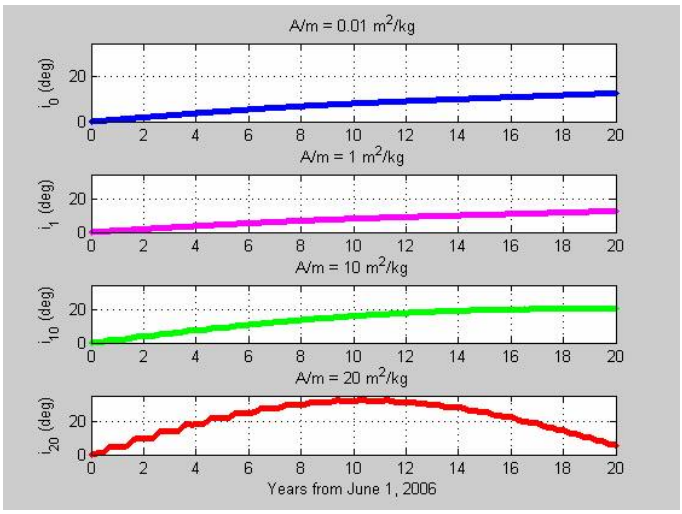

Figure 3 Inclination 20-year Histories for A/m = .01, 1, 10 and 20 m^2/kg

Focus of this Work

Though sporadic tracking coverage on many of these debris objects creates a challenge to the orbit determination, the chief problem addressed in this work is that of the apparent variation of the AMR. The AMR estimation, by way of solar radiation pressure (SRP) estimates in the orbit determination (OD) process, are seen to vary about a nominal value, as would be anticipated for a "tumbling" piece of debris. And, as one might expect, the AMR signature for each object is somewhat unique. Thus, time-varying characteristic of the AMR can create a challenge for fitting orbits to data where the solar radiation pressure (SRP) force is not constant over a fit span.

Hence, the goal of this work is to present the orbit determination analysis that has been conducted on several AMR objects being tracked by Space Command. The

inclusion of 3-dimensional process noise in the dynamic estimation of the AMR will be presented. The OD performance is summarized, with emphasis on the AMR estimation. Results are presented that indicate dynamic estimation of AMR provides improved predictions over orbit estimation where the AMR is assumed constant. Better predictions support improved tracking acquisition which, in turn, will support long-term consistent characterization of these debris objects.

TRACKING DATA HISTORIES AND ORBIT DETERMINATION PROCESS

High Area-to-mass Ratio Debris Object Summary

Tracking data for a set of 20 high AMR objects were examined to determine their orbital attributes, including the temporal characteristics of the AMR values. Data covering the period from January 1 through March 20, 2007 (approximately 10 weeks), was processed, where Space Surveillance Network (SSN) tasking provided angles-only measurements at nominally a few measurements per day. Data gaps over the period of analysis ranged from days to 10's of days. The orbital drift characteristics create periodic outages in tracking requiring predictions to support tracking reacquisition of the objects.

A summary of the objects, their nominal AMR values and J2000 classical orbital elements is given in Table 1. The AMR values for this set of debris objects range from a little less than 1 m^2/kg to just over 9 m^2/kg. All are near GEO altitudes, but with eccentricities ranging from around 0.006 to 0.3885, and inclinations ranging from about 1˚ to just over 19˚ over the period of interest. These values will change over time due to the solar radiation pressure and relatively high AMR values.

Table 1
HIGH AREA-TO-MASS RATIO DEBRIS OBJECT SUMMARY

No.	Name	AMR (m^2/kg)	Tracking Duration (days)	Sma (km)	Ecc	True Arg of Lat (deg)	Inc (deg)	RAAN (deg)	Arg of Perigee (deg)
1	Obj64	2.70410	78.38860	40401.7	0.13915	12.678	10.632	335.553	335.912
2	Obj65	1.37819	57.76943	42255.9	0.04010	218.859	14.920	358.283	345.379
3	Obj67	1.58457	74.68585	41578.1	0.03450	53.627	12.944	4.766	116.750
4	Obj68	0.97329	62.40398	40788.8	0.03086	331.349	13.313	0.450	324.960
5	Obj71	1.32969	76.92446	41451.9	0.01305	144.225	13.729	348.187	237.976
6	Obj72	7.08928	78.22507	40771.9	0.13026	1.074	18.727	324.119	145.948
7	Obj73	0.56965	78.11069	40290.1	0.05233	21.052	12.137	357.953	167.042
8	Obj74	1.05721	49.73567	42558.6	0.05056	71.116	14.635	9.167	271.145
9	Obj75	9.01183	74.71384	39350.3	0.38853	132.912	1.277	3.380	322.300
10	Obj76	1.11561	78.69614	42032.0	0.00611	8.388	14.403	358.108	335.896
11	Obj77	2.75974	65.80827	41426.3	0.05176	336.985	13.870	345.230	247.276
12	Obj80	4.25155	69.50164	41841.9	0.07353	121.373	9.385	329.734	340.159
13	Obj82	3.18572	76.40952	39717.7	0.06549	345.600	9.705	336.041	241.895
14	Obj83	2.66031	74.48047	44721.7	0.10363	60.818	16.848	358.308	350.340
15	Obj84	1.26090	78.34826	41931.8	0.00524	17.123	14.313	357.159	311.056
16	Obj85	0.79771	65.44226	42440.4	0.04033	198.708	14.739	358.973	17.519
17	Obj86	3.40915	52.95055	42450.6	0.09703	53.823	15.707	4.648	280.041
18	Obj87	4.70599	65.73438	33184.4	0.34519	15.298	8.100	72.140	243.709
19	Obj88	1.96555	73.36619	42260.2	0.07160	343.748	15.061	358.282	104.454
20	Obj99	1.92097	74.05110	44627.6	0.09770	131.951	19.129	11.684	346.958

Orbit Determination Process

An OD process was developed to provide high AMR object tracking and prediction products that could be used to support acquisition and tracking campaigns by international collaborators. The orbital dynamics result in observation phasing that truly requires continuous global coverage to insure that the objects are not "lost." The estimated state consists of position and velocity information, and a solar radiation pressure coefficient "factor" that effectively estimates a measure of the area-to-mass ratio. The consistent tracking coverage assures consistent measurements that can be used to characterize the object properties and orientation-dependent dynamics.

The Orbit Determination Tool Kit (ODTK©) was used to process a "real-time" implementation of the state estimation. ODTK© utilizes a Kalman filter based approached to the estimation, and so a state estimate is provided at each measurement update, hence, a time history of each estimated parameter is available. This includes the capability to provide SRP estimates with each measurement update and, hence, to provide insight into the AMR dynamics that might occur over a data series, and also to improve the orbit estimates. In particular, the potential time variability of the AMR parameter is of interest. Furthermore, the filtered state can be smoothed "backwards" over a specified data span to provide an optimal state estimate that reduces the uncertainty over that produced by the real-time filter. The filter parameters are saved after the latest update, and so after a measurement outage, the state is automatically propagated to the new measurement time, and proceeds with the filter update as long as data from a pass is available. Most noteworthy is that the ODTK© Kalman filter implementation allows AMR to be estimated with each measurement update, and so characterization of the time history is possible. This will be demonstrated in the results presented in the following sections.

The OD analysis for each of the objects followed the following process:

1. Perform the initial orbit determination and/or initial least-squares to determine the initial state
2. Do an initial filter/smoother pass through data with high a priori state covariance, and where needed, dynamic measurement editing
3. Examine residuals, position consistency, and AMR average estimate, and revise filter covariance and editing parameters as appropriate
4. Adjust AMR and associated sigma's, including ecliptic north and ecliptic plane fractions, and re-run the filter/smoother
5. When the AMR estimate is stable, update initial position and velocity state and covariance with the smoother state estimate, and re-run
6. Determine AMR average, variability, position consistency and error growth over data gaps

Solar Radiation Pressure and Area-to-mass Ratio Modeling

In addition to earth, lunar and solar gravitation, the solar radiation pressure (SRP) is a significant force affecting the orbital dynamics of GEO objects. Objects having high AMR are particularly susceptible to solar force acceleration. The solar radiation acceleration is[3]

$$\vec{a}_{radiation} = \frac{p_{SR} c_R A_S}{m} \hat{r}_S \quad \textbf{(1)}$$

where

p_{SR} = solar radiation pressure
c_R = solar pressure parameter
A_S = effective area facing sun
m = object mass
$\hat{r}_S$ = vector from object to sun

In most OD implementations a nominal value of c_R is typically specified, and a fixed correction estimated as part of the batch least squares state solution. The values of A_S and m are usually specified if those properties are known, and the values of p_{SR} and $\hat{r}_S$ are computed based on the orbital geometry relative to the sun. In the absence of physical information of the object properties, the combined quantity of

$$\gamma = \frac{c_R A_S}{m} \quad \textbf{(2)}$$

can be estimated. If c_R is assumed to be equal to 1, then the OD process is effectively estimating A_S/m. For the batch least square implementation, the A_S/m is estimated as a constant over the fit span. This limitation can have a significant effect if A_S/m varies significantly over the time scale of the fit span. Note that mass is assumed fixed, and so A_S/m variations are really just an indication of the object orientation changes resulting in variation of the cross sectional area exposed to the sun. All discussions of AMR throughout this work are taken to be synonymous with SRP.

In addition to the ability to estimate the AMR with each measurement update, ODTK© allows for the incorporation of white process noise into the estimate, not only along the sun-to-satellite line, but in two components specified via the Ecliptic North Fraction and the Ecliptic Plane Fraction normal to the sun-to-satellite line. This is useful when significant solar pressure accelerations exist in these directions, since the standard solar pressure model alone cannot account for such accelerations.

Process noise along the sun-to-satellite line is added when the solar pressure coefficient is estimated. For the Ecliptic North Fraction, f_N, the acceleration noise is added in the direction normal to the sun-to-satellite line and normal to the ecliptic plane. It is computed as the magnitude of the nominal solar pressure acceleration multiplied by f_N. For example, to add white noise equal to 50% of the nominal acceleration in the Ecliptic North direction, specify a value of 0.5. For the Ecliptic Plane Fraction, f_P, the acceleration noise is added in the direction normal to the sun-to-satellite line and co-planar to the ecliptic plane. It is computed as the magnitude of the nominal solar pressure acceleration multiplied by the f_P. For example, to add white noise equal to 50% of the nominal acceleration in the Ecliptic Plane direction, specify a value of 0.5.

A measure of the magnitude of the solar radiation pressure can be defined as the ratio of the acceleration magnitude and solar pressure

$$\frac{|\bar{a}_{radiation}|}{p_{SR}} = \frac{A_S}{m}\sqrt{1 + f_N^2 + f_P^2} \tag{3}$$

McReynolds' Filter-Smoother Consistency Test

The performance of the Kalman filter, and the subsequent smoothing of the filter solutions, can be measured according to the consistency of the measurement corrections relative to the updated covariance. A measure of filter-smoother performance, known as the "McReynolds' consistency test", can be summarized by defining the following[4]:

X_k^f = filtered state estimate at time t_k

X_k^s = smoother state estimate at time t_k

P_k^f = filtered covariance estimate at time t_k

P_k^s = smoother covariance estimate at time t_k

then compute the estimated state and covariance differences between the filter and smoother:

$$X_{\Delta k} = X_k^f - X_k^s \tag{4}$$

$$P_{\Delta k} = P_k^f - P_k^s \tag{5}$$

Then for, the i^{th} element of $X_{\Delta k}$ and the square root of the i^{th} element of $P_{\Delta k}$, define the ratio

$$R_k^i = \frac{X_{\Delta k}^{\ i}}{\sigma_{\Delta k}^{i}} \tag{6}$$

If abs(R^i_k) ≤ 3 for all i and k, then the test is satisfied globally for each estimate. If abs(R^i_k) > 3 for all i and k, then the filter-smoother test fails globally indicating the possibility of mis-modeling. Thus, position, velocity and AMR estimation performance can be assessed in terms of the ratio of the estimates to the predicted/assumed modeling uncertainties.

Detailed Orbit Determination Performance Results for Object 84

The detailed OD results are presented for debris Object 84 to illustrate an example where the AMR appears to exhibit periodic behavior, as data for this object were available over a 14 month period. The residual ratios, the ratio of the absolute residual to the tracking sensor measurement σ (nominally a few arc-seconds) is shown in Figure 4, where it can be seen that most of the residuals are less than the 3-σ level indicated by the black horizontal lines.

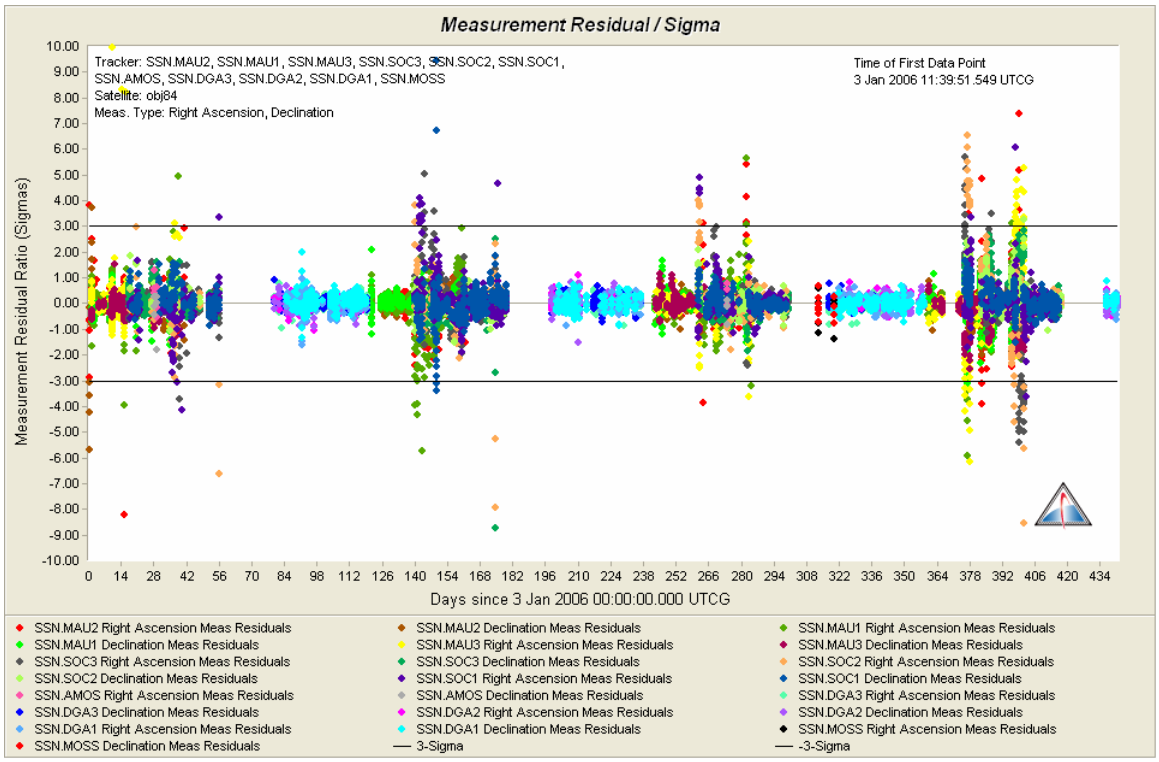

Figure 4 Residual Ratios for Object 84

The filter position and velocity radial, in-track and cross-track (RIC) 1-σ uncertainties are shown in Figures 5 and 6, where the radial position uncertainties are seen to be larger than the in-track and cross-track uncertainties, consistent with angles-only OD processing which typically provides poor observability in the radial direction.

Note also the correlation between the larger in-track velocity uncertainties. The process noise added to the SRP in the AMR estimation is also a factor that drives the distribution of weighting in the Kalman filter estimates. The various data gaps over the period can also be seen in the plots where the uncertainty in each RIC component grows during measurement outages in a "saw-tooth" fashion. In this case, the radial position uncertainty does not exceed 60 km during any one outage over the 14-month period.

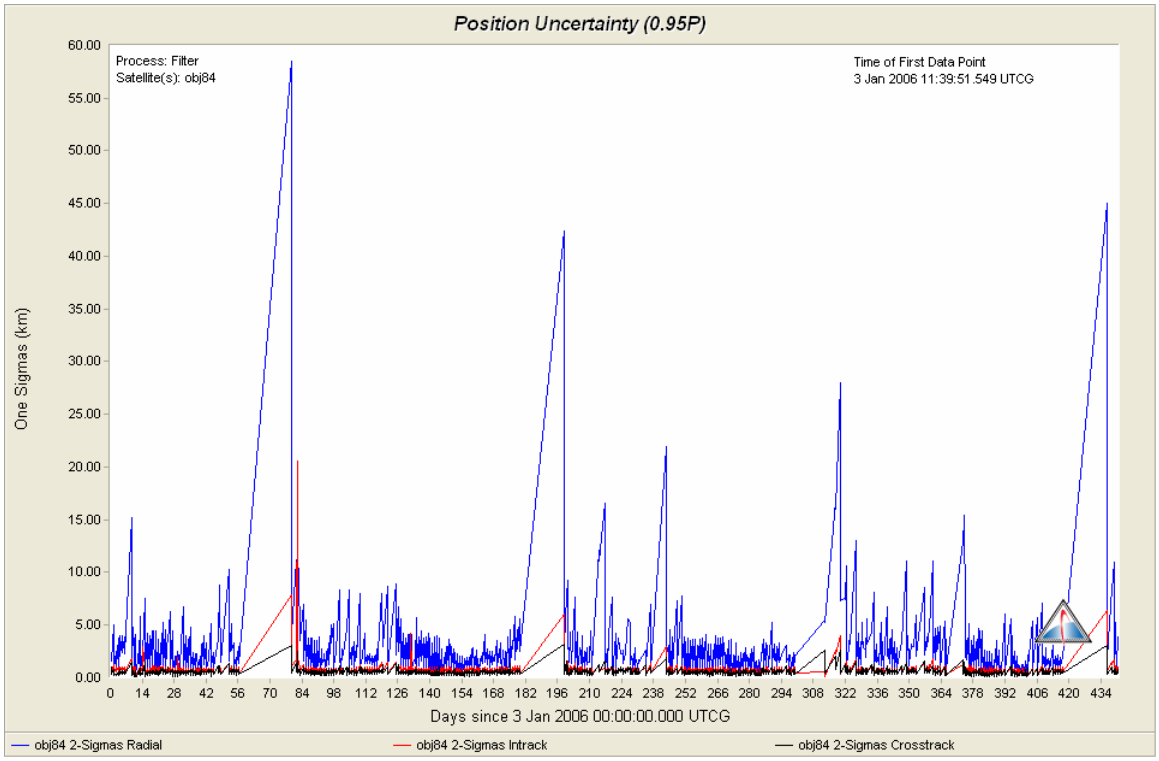

Figure 5 RIC Position Uncertainty for Object 84

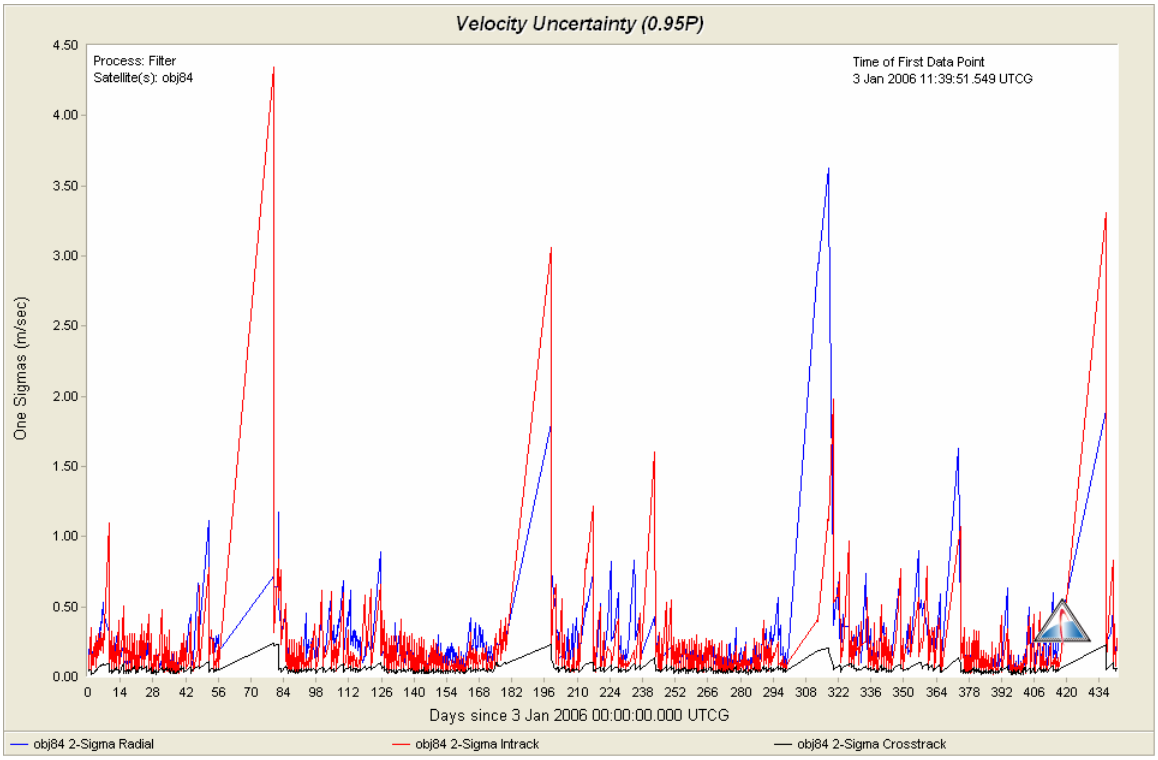

Figure 6 RIC Velocity Uncertainties for Object 84

The AMR estimation corrections over the 14 month period are shown in Figure 7, where the variations exhibit a clear periodic pattern of relatively quiescent segments interspersed with periodic elevated values. The higher amplitude estimates are a factor of 10 or more larger than the quiescent amplitudes, with those episodes occurring at a period of around 112 days. These variations in AMR are what might be expected for a "tumbling" piece of debris, and though the AMR signatures for each object are somewhat unique, at least some of them may be amenable to modeling. This time-varying characteristic of the AMR creates a challenge for fitting orbits to data where the solar radiation pressure (SRP) force is not constant over a fit span.

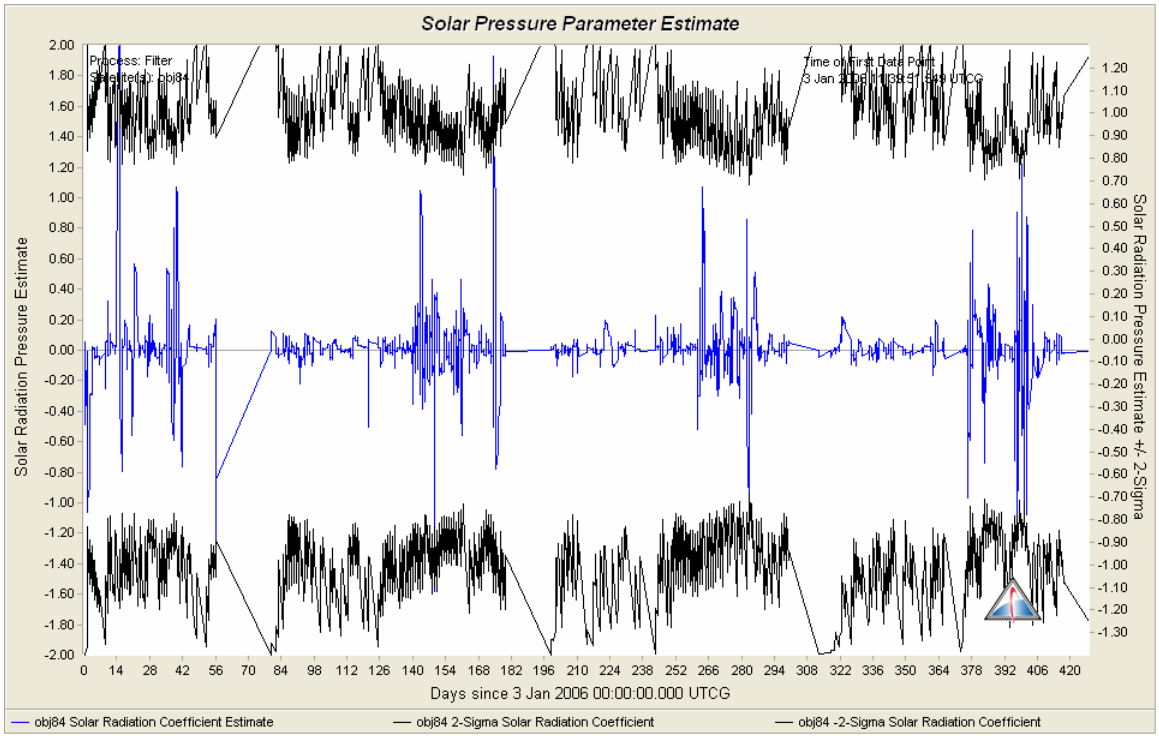

Figure 7 AMR Estimate for Object 84

The filter processes the "optimum state estimate" at each measurement update. In a sequence of measurements over a relatively short period of time relative to the process noise half-life, the state estimation uncertainty gets smaller, i.e. estimation knowledge improves. The result is that the state history typically contains changes that reflect this change in uncertainty, and not the physics. The smoothing process takes the state estimates and back estimates and back-processes over the data to resolve this physical inconsistency. The smoothed states are akin to batch least squares results, though dynamic parameters such as the AMR are still allowed to vary. The filter versus smoother differences can be thought of as a measure of the propagation errors between measurements, as the filtered state is somewhat independent of the "global knowledge" of the data that the smoothed state posses. The filtered versus smoothed stated differences for Object 84 over the 14-month series are shown in Figure 8, with the predominant radial errors varying between ±10 km, and the in-track and radial vary between ±2 km.

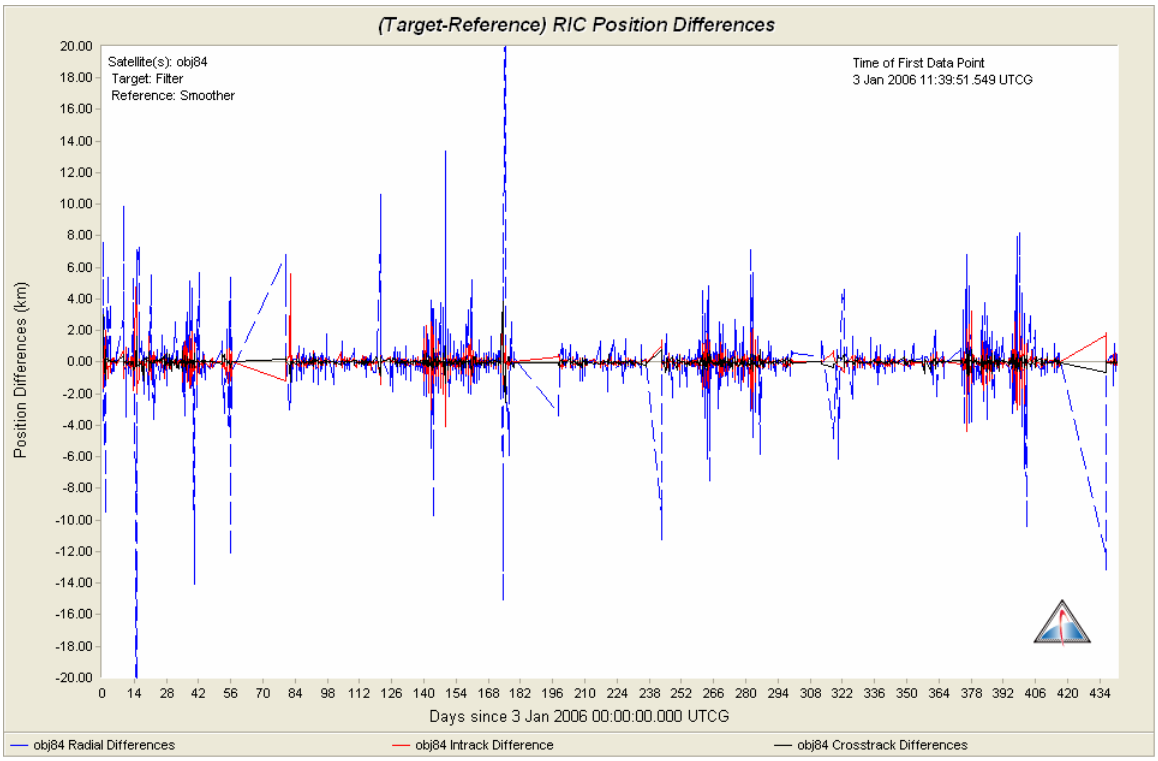

Figure 8 RIC Filter-Smoother Differences for Object 84

The position and AMR filter-smoother RIC position and AMR consistency values, as defined in equation (6), are plotted in Figures 9 and 10, respectively. Though they are nominally less than 3, anomalies occur in the neighborhood of the elevated AMR estimates indicating the perhaps the corrections are larger than the modeling uncertainties anticipate. The *a priori* σ and process noise applied to the AMR estimates are fixed over a given process run. To obtain consistency throughout the series, these would need to vary dynamically in order to reflect the physics driving variations from low to high amplitude forces acting on the debris.

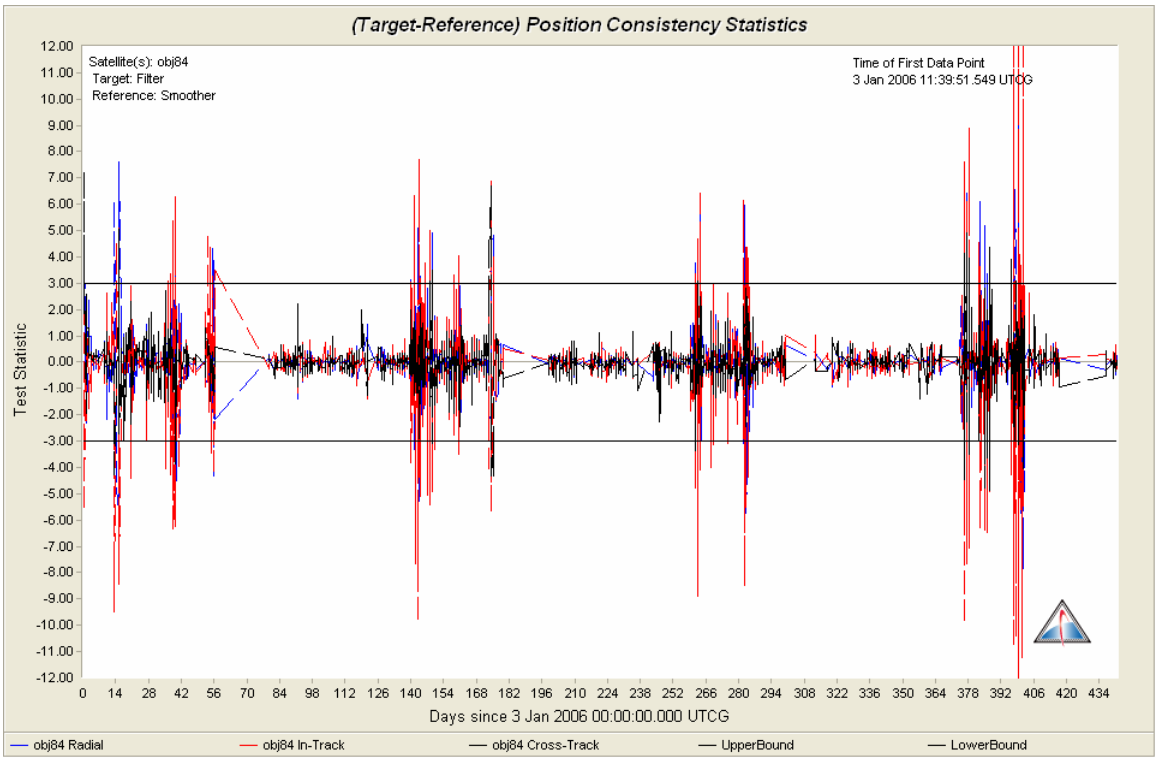

Figure 9 Position Consistency for Object 84

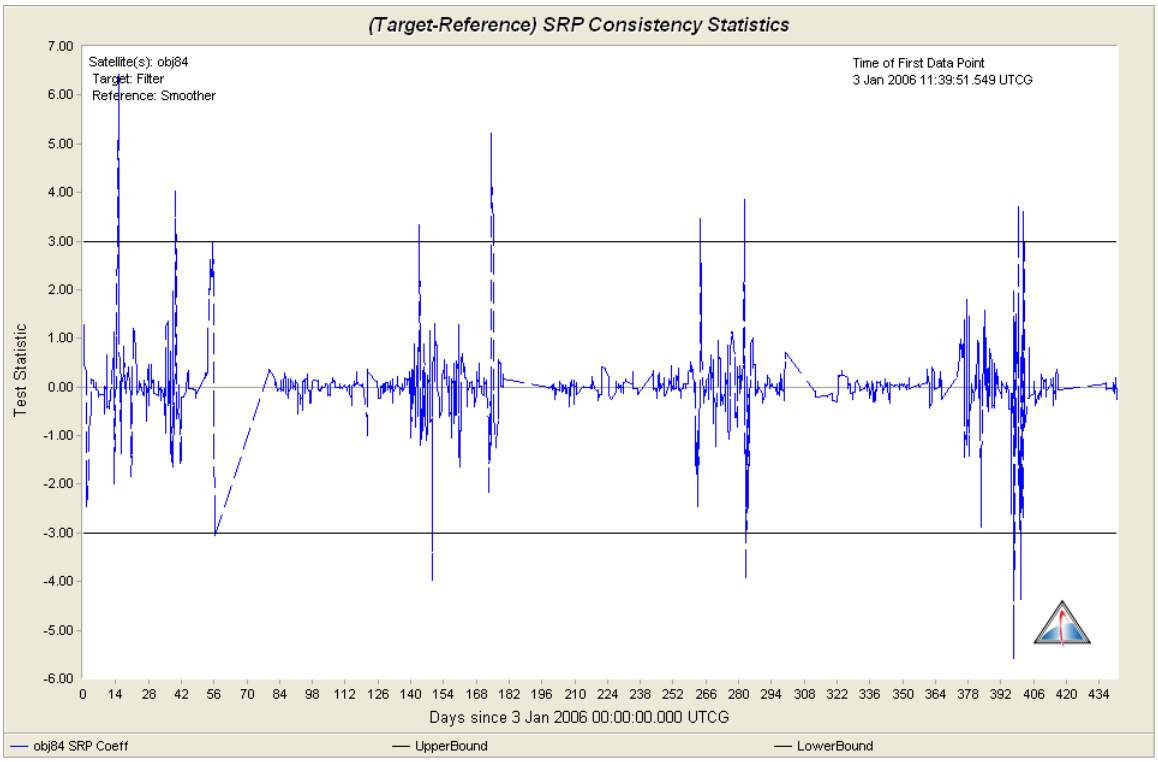

Figure 10 AMR Consistency for Object 84

Orbit Determination Summary for 20 Debris Objects

A summary of the OD results for the 20 objects is provided in Table 2. The σ_{Am} is the 1-σ variation of the AMR estimates over each of the given series, relative to the average AMR value listed. The fractional variation is the ratio of σ_{Am} relative to the AMR, and can be seen to range from a few percent to several hundred percent for Object 73. The ecliptic north and ecliptic plane fractions are the values used in the solutions to each of the given objects, while the "AMR Mag Factor" is the total magnitude as defined in equation (3). The ecliptic north and plane values were determined by trial-and-error such that the postion/velocity and AMR consistency values were optimized to below 3. The "AMR Variation" is the effective total variation based on the magnitude factor and the variation of the AMR estimates. The "RSS Pos" and "RSS Vel" are the root-sum-squared (RSS) of the position and velocity filter-smother differences over the time histories, where the position errors range from a few kilometers to a few 10's of kilometers. These errors represent a measure of the prediction error growth in between measurement updates, where the outages range from days to 10's of days. Finally, the RSS Pos/Vel Consistencies are the root-sum-squared position and velocity consistencies for each of the objects over the time history. Each RIC component of the position and velocity solutions was less than 3 and, hence, the RSS's are less than 9 (3-squared). In all cases, the AMR filter-smoother consistencies were less than 3.

Table 2
ORBIT DETERMINATION SUMMARY

No.	Name	AMR (m^2/kg)	σ_{Am} (m^2/kg)	Fractional Variation	Ecliptic North f	Ecliptic Plane f	AMR Mag Factor	AMR Mag Variation	RSS Pos Differences (km)	RSS Vel Differences (m/s)	RSS Pos Consistency	RSS Vel Consistency
1	Obj64	2.70410	0.95719	0.3540	4.00	8.00	24.34	8.61	15.1259	2.11080	3.56	2.12
2	Obj65	1.37819	0.90009	0.6531	1.00	3.00	4.57	2.99	43.3098	3.96441	3.69	3.88
3	Obj67	1.58457	0.30244	0.1909	1.00	0.00	2.24	0.43	3.0401	0.36157	2.74	2.50
4	Obj68	0.97329	0.37018	0.3803	8.00	4.00	8.76	3.33	5.3159	0.69861	2.00	2.00
5	Obj71	1.32969	0.71748	0.5396	1.00	1.00	2.30	1.24	12.4169	1.20913	4.36	4.88
6	Obj72	7.08928	0.43919	0.0620	1.00	0.10	10.05	0.62	3.5999	0.69111	3.88	3.74
7	Obj73	0.56965	1.37380	2.4117	2.00	2.00	1.71	4.12	28.8034	2.11768	3.31	3.36
8	Obj74	1.05721	0.45688	0.4322	1.00	4.00	4.49	1.94	13.9899	1.13109	3.34	3.46
9	Obj75	9.01183	0.22468	0.0249	6.00	0.10	54.82	1.37	26.7959	2.76661	4.22	2.86
10	Obj76	1.11561	0.06072	0.0544	1.00	0.50	1.67	0.09	5.7517	0.53919	1.30	1.13
11	Obj77	2.75974	0.54668	0.1981	1.00	2.00	6.76	1.34	37.3793	2.76812	3.47	3.59
12	Obj80	4.25155	0.55736	0.1311	1.00	0.10	6.03	0.79	6.6489	0.53050	2.56	2.37
13	Obj82	3.18572	0.06599	0.0207	1.00	0.50	4.78	0.10	1.4135	0.18561	2.26	2.46
14	Obj83	2.66031	0.19541	0.0735	0.00	0.00	2.66	0.20	2.4564	0.17941	2.85	2.97
15	Obj84	1.26090	0.19900	0.1578	1.50	0.70	2.44	0.38	2.8994	0.24954	2.88	2.75
16	Obj85	0.79771	0.34596	0.4337	1.00	1.00	1.38	0.60	5.0536	0.89720	3.58	2.23
17	Obj86	3.40915	0.09793	0.0287	0.50	0.10	3.83	0.11	1.5540	0.12160	1.85	1.85
18	Obj87	4.70599	0.20236	0.0430	2.00	0.10	10.53	0.45	1.5127	0.17240	2.14	2.15
19	Obj88	1.96555	1.00570	0.5117	2.00	2.00	5.90	3.02	35.5549	2.71422	3.87	3.39
20	Obj99	1.92097	0.18357	0.0956	0.30	0.00	2.01	0.19	2.3334	0.20288	2.21	2.06

The position and velocity differences plotted versus the AMR magnitude variations are shown in Figures 11 and 12. The plots indicate some correlation between the errors and AMR variations. As one might expect, the error growth over the outages between measurement updates is related to the AMR variations, where larger AMR variations result in larger propagation errors. Though not shown, the distribution of the errors amongst the RIC components had the largest errors in the radial component, with in-track having the next largest, and the cross-track being the lowest.

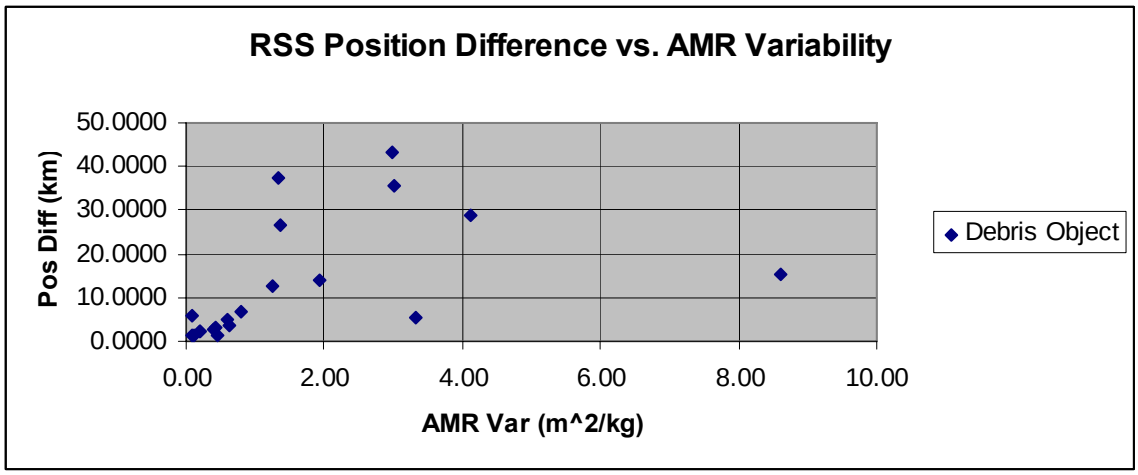

Figure 11 Position Error vs. AMR Variation

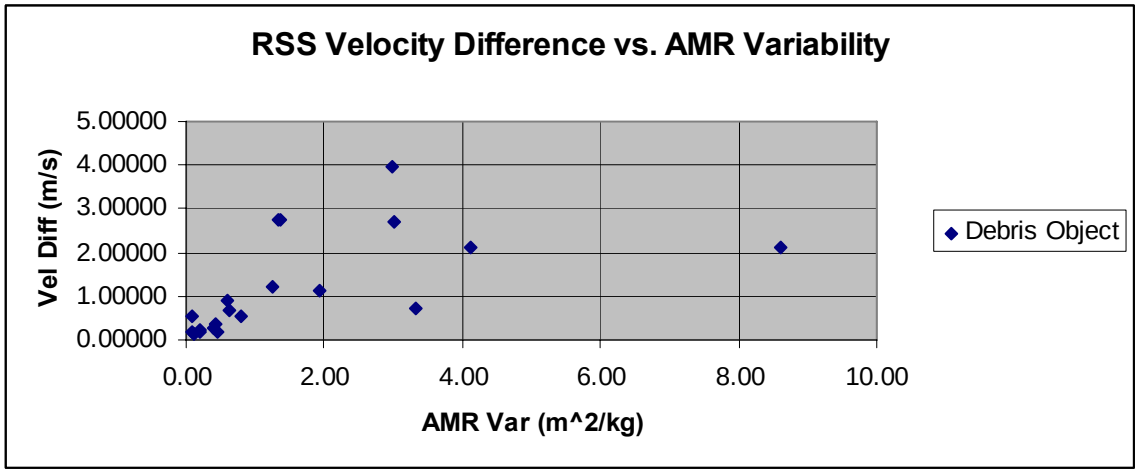

Figure 12 Velocity Error vs. AMR Variation

PREDICTION ERROR ANALYSIS

The typical optical sensor field-of-view (FOV) is on the order of 1˚ or less[5], which at GEO ranges translates into acquisition errors on the order of 700 km or less in the sensor plane. The orbit prediction error at sensor acquisition must be less than this when mapped into the sensor FOV plane, or a search strategy will need to be initiated. It is of interest, then, to examine criteria for obtaining the best prediction results.

A 34 day segment of the tracking data for Object 84 which contains a 20-day measurement gap was examined to determine the sensitivity of prediction performance to the AMR estimation strategy. The residual ratios for this span are shown in Figure 13, and are well below the 3-σ level.. The propagated state derived from the filter update is compared to a propagated stated derived from a batch least-squares solution state propagated over the 22-day gap. In each case a consistency difference performance metric is used where the overlapping prediction state differences are examined.

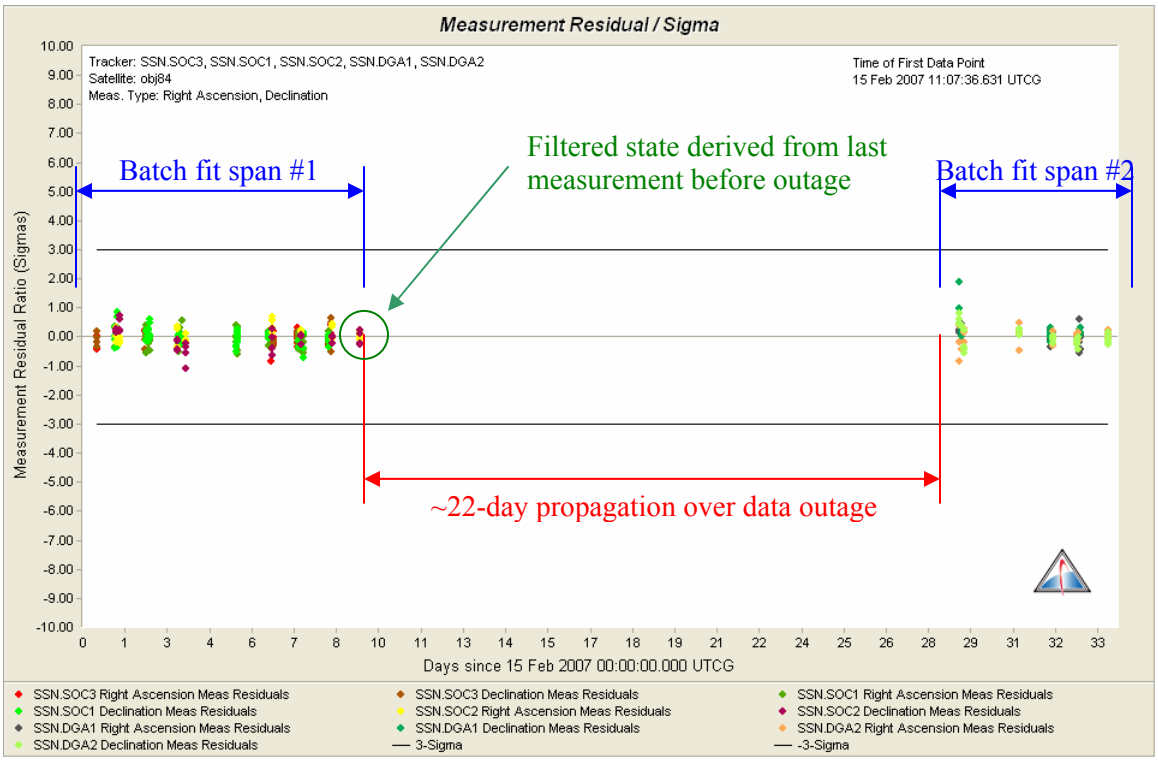

Figure 13 Object 84 Residual Ratios over 20 Day Measurement Gap

The AMR (solar pressure) correction estimates from the Kalman filter solutions are seen in Figure 14 to vary by a few percent relative to the nominal value of 1.2609 m^2/kg. Noteworthy is the slight bias of less than 1% in the averages of the two segments. This 34-day segment corresponds to the relatively quiescent piece at the very end of the 14 month time history shown in Figure 7.

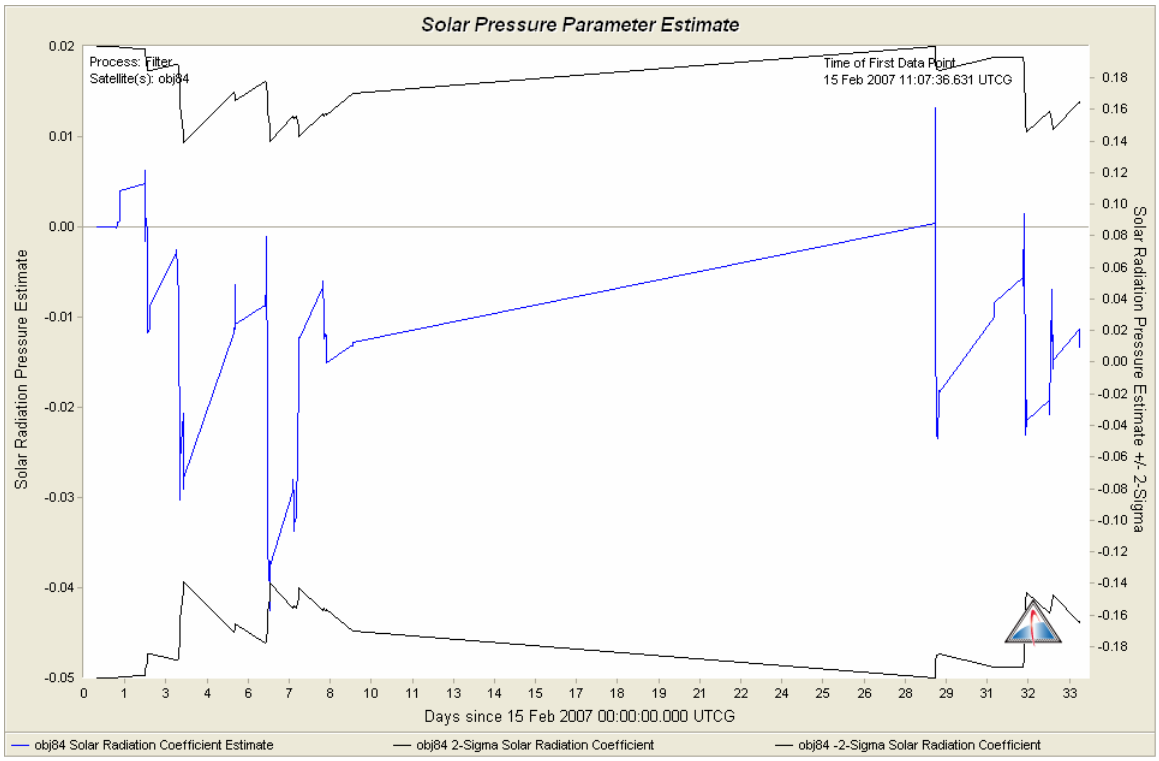

Figure 14 Object 84 AMR Estimates over 20 Day Measurement Gap

The propagation RIC error growth in the case where the initial propagation state is taken from the last filter update prior to the outage is shown in Figure 15. In this case, the filtered position (and velocity) states were compared to the smoothed states. The maximum error is seen to be in the radial component, and reaches around -8 km over the 20-day outage. The in-track and cross-track errors each grow to less than 1 km in magnitude. The radial error is the result of poor observability in that component due to the nature of angles-only measurements. Experiments were conducted in this analysis that showed greater in-track error growth when the AMR was not properly modeled as indicated by poor position and AMR consistency results.

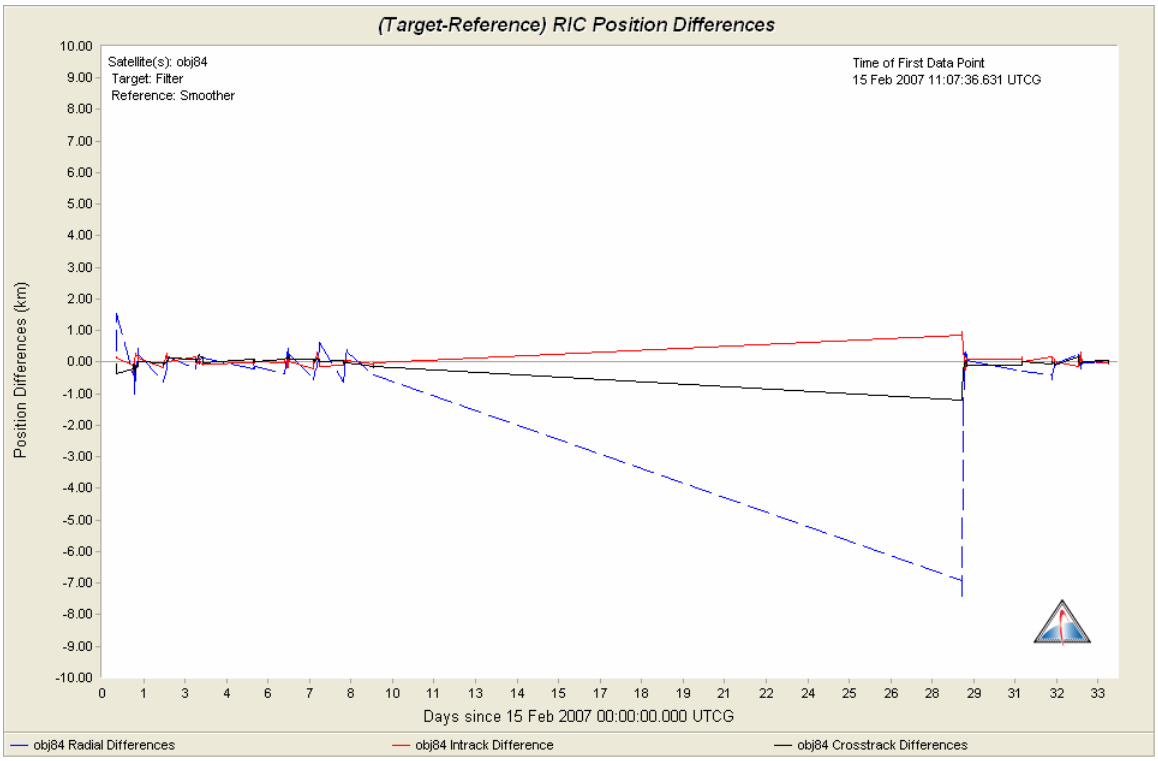

Figure 15 RIC Filtered Position Prediction Error for Object 84 – Estimated AMR

To examine the propagation errors based on a batch least-squares orbit solution, the two data segments shown in Figure 13 were estimated independently, and independent, fixed AMR values were estimated for each of the two segments. The resulting estimated states for each segment were used to propagate those states such that they overlapped in time. The overlap RIC differences are shown in Figure 16. The differences at the far left of the graph correspond to the end of the data outage. It can be seen that the in-track error is around -50 km at that point, and grows beyond that with time. The radial and cross-track errors are periodic with amplitudes less than 10 km. Thus, even for this quiescent segment, the dynamic estimation of AMR appears to provide significant improvement in the prediction results. Period of elevated AMR variability would likely widen this performance gap.

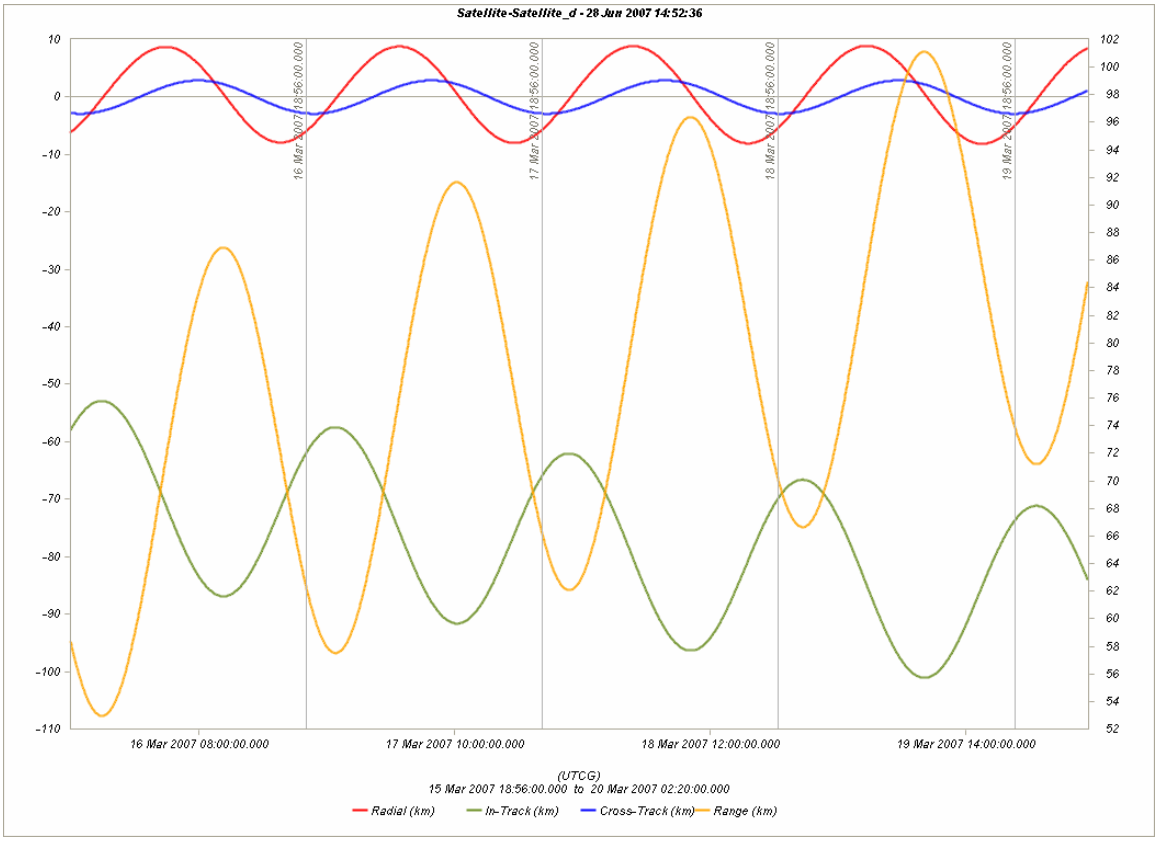

Figure 16 RIC Batch Position Prediction Error for Object 84 – Independent Fixed AMR Values Estimated for Each of the Two Fit Segments

CONCLUSION

The orbit determination analysis indicates that the AMR variations are not always consistent for a given debris object, and can have significant "spikes" over certain periods likely to be orientation-dependent. The best results are achieved when process noise is added to the AMR, not only along the sun line, but in directions orthogonal to the sun line (ecliptic plane and ecliptic north directions). Appropriate bounding of the AMR via the *a priori* σ for that parameter accommodates the "nominal" variations, and translates into more realistic state covariance values for the estimated position/velocity state. If periodic behavior is noted in the AMR estimates, the parameter can be modeled to produce more accurate predictions. RIC error growth rate for given object is correlated to the magnitude of the variability of that object's AMR. The orbit determination results were presented for several of these debris objects, and highlight their unique and varied dynamic attributes. Results presented here indicate a correlation between the AMR variation and prediction errors. Furthermore, if the AMR is estimated as fixed over short periods, there can still be significant prediction error growth compared to AMR values estimated dynamically. Future efforts will focus on analytical means to more precisely quantify the AMR variations in terms of any possibly periodicities, and development of AMR models that might incorporated into the dynamic modeling of SRP to improve the orbit predictions.

ACKNOWLEDGEMENT

We would like to acknowledge the NASA Orbital Debris Program Office for supporting the analysis presented here, the U.S. Air Force Space Command for providing tracking data for the debris objects so crucial to this work, Dick Hujsak at AGI for ODTK© consulting support, and the late John Africano for inspiration and more. John made it all happen, and in some instances, he still does.

REFERENCES

1. Schildknecht et al., Properties of the High Area-to-mass Ratio Space Debris Population in GEO, AMOS Tech. Conf. 2005.
2. Anselmo, Luciano and Carmen Pardini, "Long-Term Simulation of Objects in High-Earth Orbits," Space Flight Dynamics Laboratory, Pisa, Italy, ESA/ESOC Contract to ISTI/CNR Report, Contract No. 18423/04/D/HK, 13 December, 2006.
3. Vallado, David A., "Fundamentals of Astrodynamics," Second Edition, Microcosm Press, 2001.
4. Wright, James, "Optimal Orbit Determination," Analytical Graphics, Inc., internal white paper, 2002.
5. Schildknecht, Thomas, "Optical surveys for space debris," Astronomy and Astrophysics Review, SOI 10.1007/s00159-006-0003-9, Springer-Verlag, 9 January 2007.